Open Access

Journal of Energy and Power Technology

LIDSEN Publishing Inc.

Research Article

Synthetical Optimal Design for Passive-Damped LCL Filters in Islanded AC Microgrid

Xiuhui Tang, Daming Zhang *, Hua Chai

School of Electrical Engineering and Telecommunications, University of New South Wales, Kensington, Sydney, NSW 2052, Australia; E-Mails: xiuhui.tang1@unsw.edu.au; daming.zhang@unsw.edu.au; hua.chai@unsw.edu.au

* **Correspondence:** Daming Zhang; E-Mail: daming.zhang@unsw.edu.au

Academic Editor: Zhao Yang Dong

Journal of Energy and Power Technology
2021, volume 3, issue 3
doi:10.21926/jept.2103032

Received: May 19, 2021
Accepted: July 04, 2021
Published: July 08, 2021

Abstract

In AC microgrid systems, technical issues resulting from the power control effect are the power control method efficiency and the filter resonance since voltage-frequency interference and filtering resonance may cause significant control input reduction and oscillation. A simple and robust solution is to regulate active power flow by adding an optimal passive damping resistor. The optimal LCL filter parameterization process in this paper provides an innovative approach to obtain the optimal quality factor and the optimal damping resistor. The amplitude responses of resonant frequency and high frequency are involved in the cost function. Simulations of various cases are conducted in MATLAB/Simulink. The key advantages of this procedure include flattened admittance peak, weakened high frequency decay, and less damping loss. Through the method in this paper, the optimal passive-damped filter parameters can be calculated in an efficient manner, while the power can be regulated and tracked in a simplified way, and the performance of the control strategy is improved.

Keywords

LCL filter; passive damping; optimal parameterization

1. Introduction

With the imminent depletion of fossil fuel, maximally harnessing renewable energy becomes indispensable. If all the renewable energy is tapped into existing power grid, a severe instability could occur due to intermittence of solar or wind energy generation. Autonomous microgrid can be taken to cope with instability of large power grid and intermittence of renewable generation. In the meantime, the maximum power extraction from solar and wind can still be implemented in such a system. This research aims to design of passive filters with passive damping and use of such a design in operation of islanded microgrid. The purpose of introducing high-order filters into microgrids is to have better damping and smoothing effect so that the size and cost of the filter will be reduced. A commonly used high-order filter is the LCL filter, which is often used in ports connected with the main power grid after the output of various power supplies [1-9].

However, the resonance peak (peak point of resonance frequency) changes as the reactance of the system varies. This requires some active and/or passive circuits to ensure the stability of the current control system after the inverter [10]. It is now widely known that the existing control system no longer requires any attenuation when the resonant frequency of the LCL filter is greater than the critical resonant frequency. However, the stability of the inverter-based microgrid system largely depends on the internal impedance of the circuit [11].

When the electrical components of the grid are fixed but unknown, it is necessary to add attenuation to reduce the filter resonance and remove the oscillation effect of the renewable energy system connected to the inverter on the main grid [1, 12]. Although there are active and passive damping options, active damping increases the number of sensors and observers in the system [1, 13-16]. At the same time, the stability and robustness of the system will become extremely complicated because the active damping seriously increases the order of the control system. However, passive damping can be in series or parallel on the LCL filter itself. The high frequency attenuation can be significantly suppressed without undue influence on stability and energy loss [5].

Although there are ways of designing passive damping in the previous literature [17-19], the optimal way to choose is not clear and coherent. Many methods proposed in the literature fix the magnitude of the damping resistance, but the actual resonance in the circuit is uncertain [20-23]. It is impractical to calculate the damping system parameters in an authentic microgrid system.

Therefore, this paper provides a comprehensive method for designing high-order filters. A method to find the optimal resonant frequency is designed to weaken the peak resonant frequency. Compared with previous methods, this method has the advantage of being more straightforward and more intuitive. At the same time, it ensures the effective search of resonant frequency, the maximum weakening of the resonance peak at the frequency, the use of small damping elements, and also small energy loss. For high frequency band, the attenuation is dramatically restrained at the same time [24-31].

The overall structure of this paper is as follows. First, the features of the filter are introduced, and the design constraints of the filter are determined. After discussing the proposed optimal damping design method, each step of the optimal design is presented. The control and synchronization methods of the microgrid system are also described. Finally, the conclusion of the simulation results is discussed.

2. Filter Design

A conventional LCL filter consists of an inverter-side inductor, load-side inductor, and shunt capacitor, as in Figure 1. For a practical inductor, it is always accompanied by a non-zero small series resistor. To achieve the passive damping properly, a capacitor with large equivalent series resistance (ESR) can be used. Or an extra resistor is added in series with the capacitor with small ESR [19, 32-34].

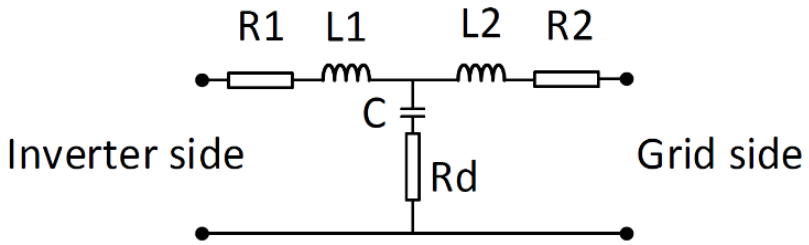

Figure 1 LCL filter with different resistor positions.

However, this series resistance will change the transfer function of the filter along with the poles and zeros, resulting in different system response effects, shown in Table 1.

Table 1 LCL Admittance structure.

Resistor position	Admittance
No R	$Y(s) = Y_0(s)\dfrac{1}{\dfrac{s^2}{{w_0}^2}+1}$
R_1 in series	$Y(s) = Y_0(s)\dfrac{1}{\dfrac{s^2}{{w_0}^2}+\dfrac{R_1 s}{L_1{w_0}^2}+R_1Y_0(s)+1}$
R_d in series	$Y(s) = Y_0(s)\dfrac{R_dCs+1}{\dfrac{s^2}{{w_0}^2}+R_dCs+1}$
R_2 in series	$Y(s) = Y_0(s)\dfrac{1}{\dfrac{s^2}{{w_0}^2}+\dfrac{R_2 s}{L_2{w_0}^2}+R_2Y_0(s)+1}$

Now it is specified L_1 to be inverter side inductor, L_2 to be line side inductor, and C to be filter capacitor. They have the following computational relationship:

$$Y_0(s) = \frac{1}{s(L_1+L_2)} \tag{1}$$

$$w_0 = \frac{1}{\sqrt{L_1L_2}} \tag{2}$$

$$L = \frac{L_1 L_2}{L_1 + L_2} \tag{3}$$

2.1 Passive Filter

Filter structures shown in Figure 2 are LCL filter without passive damping and LCL filter with damping resistor in series with a capacitor.

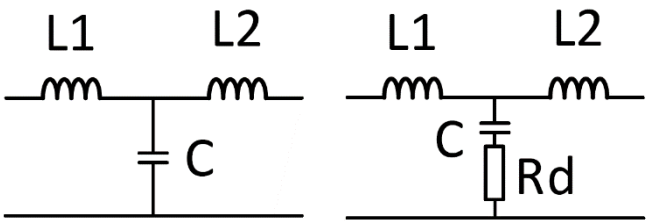

Figure 2 LCL filter without and with a damping resistor R_d.

The transfer functions for LCL and LCL+R_d filters are:

$$Y_{LCL}(s) = \frac{1}{L_1 L_2 C s^3 + (L_1 + L_2)s} \tag{4}$$

$$Y_{LCL+R}(s) = \frac{CR_d s + 1}{L_1 L_2 C s^3 + C(L_1 + L_2)R_d s^2 + (L_1 + L_2)s} \tag{5}$$

It is clear that the existence of the damping resistor R_d influence system stability and frequency response. The addition of zero points to the Rd of the numerator causes the oscillatory properties to change. The efficiency of the system is sacrificed to improve its stability by this passive damping. In the frequency domain, the resonance peak will be decreased to a certain degree. Also, the resonance frequency will be shifted with the design.

2.1.1 LCL Filter Design

When designing an LCL filter, characteristic frequency should be far separated from the primary harmonics of bus voltage. In the high frequency part of the frequency response, the switching ripple exhibits some decay.

These elements need to satisfy in percentage as defined in [35],

$$L_1 + L_2 \leq C \; or \; L_1 + L_2 \leq 12\% L_b \tag{6}$$

In the LCL filter, the transfer function of forward trans-admittance of the filter is in (4).

It has no zero, while pole assignment depends on LCL filter parameter selection. By transforming the form of transfer function into (7), it can be found that all the roots are related to resonance frequency except one root located at the origin.

$$Y(s) = \frac{1}{s(L_1 + L_2)(LCs^2 + 1)} \tag{7}$$

In filter design, the resonance frequency f_{res} is

$$f_{res} = \frac{1}{2\pi}\sqrt{\frac{L_1 + L_2}{L_2 L_2 C}} \tag{8}$$

And should have the relationship of (9) regarding grid frequency and switching frequency.

$$10 f_{grid} < f_{res} < 0.5 f_{sw} \tag{9}$$

The above equation implies resonance frequency should be within this limit, having some distance from the grid frequency and minimally half of the switching frequency. This makes the filter have enough attenuation. Also, it reduces resonance problems due to low frequency or switching frequency harmonics [35].

Given certain system line to line voltage V_{LL}, power rating of active power P_n and grid frequency w_n, the base impedance Z_b, base capacitance C_b and an initial trial of damping resistance could be calculated.

The LCL filter parameters could be found using:

$$Z_b = \frac{{V_{LL}}^2}{P_n} \tag{10}$$

$$C_b = \frac{1}{w_n Z_b} \tag{11}$$

$$R_d = \frac{1}{3 w_{res} C} \tag{12}$$

Voltage deviation ΔV_L is assume to be less than 10% of the voltage drop according to the IEEE 1547 standard. The maximum current ripple from the inverter output is $\Delta I_{L-max} = (1 - \mathrm{m}) * \mathrm{m} * T_{sw} \frac{2V_{DC}}{3L_1}$. When m=0.5, it is the maximum p-p current ripple. Usually, 10% ripple of the rated current is used to reduce the losses caused by switching currents in L_2. Current ripple $\Delta I_{L-max} = 0.1 * \frac{P_n\sqrt{2}}{3V_{LL}}$ to be around $5\% - 10\%$, so that the maximum grid ripple does not go more than 0.3%. For ripple current requirement, $L_1 = \frac{V_{DC}}{6 f_{sw} \Delta I_{L-max}}$ to be around $6\% - 9\%$ of Z_b. The accepted maximum power factor change from the grid side is 5%, so that $C = 5\% * C_b$. This could be larger than 5% to compensate the inductive impedance. The capacitor cannot be too small, because it might need larger inductor in order to meet the requirements of attenuation. It cannot be too large, because it increases the reactive power and rated current at the grid side. $L_2 = \frac{\sqrt{\frac{1}{{k_a}^2}+1}}{C{w_{sw}}^2}$ with desired attenuation factor k_a to be around 20%. Current THD should be lower than 5% to satisfy IEEE 519 standard [36]. The initial approximation of parameters could start from $\frac{L_1}{L_2} = 3$, later with some slight tuning.

If the above design does not meet the requirement, increase C with small steps or reduce $\frac{L_1}{L_2}$ ratio. And later repeat the design procedures. Select the option with the highest attenuation to the switching frequency component [35-41].

The overall LCL parameter design process is shown in the flow chart in Figure 3. In this design procedure, some constraints are set such as grid impedance variation, resonance frequency problems, stability issues. Then the basic power, voltage, current, frequency data is input into the calculation. When the base values are found, an initial trial of the capacitor and inverter side inductor is selected. Later some limits are checked: maximum current, current ripple, resonance frequency limit, inductance limit. Then the grid side inductor is found. Finally, the stability and performance are tested to verify this parameter design.

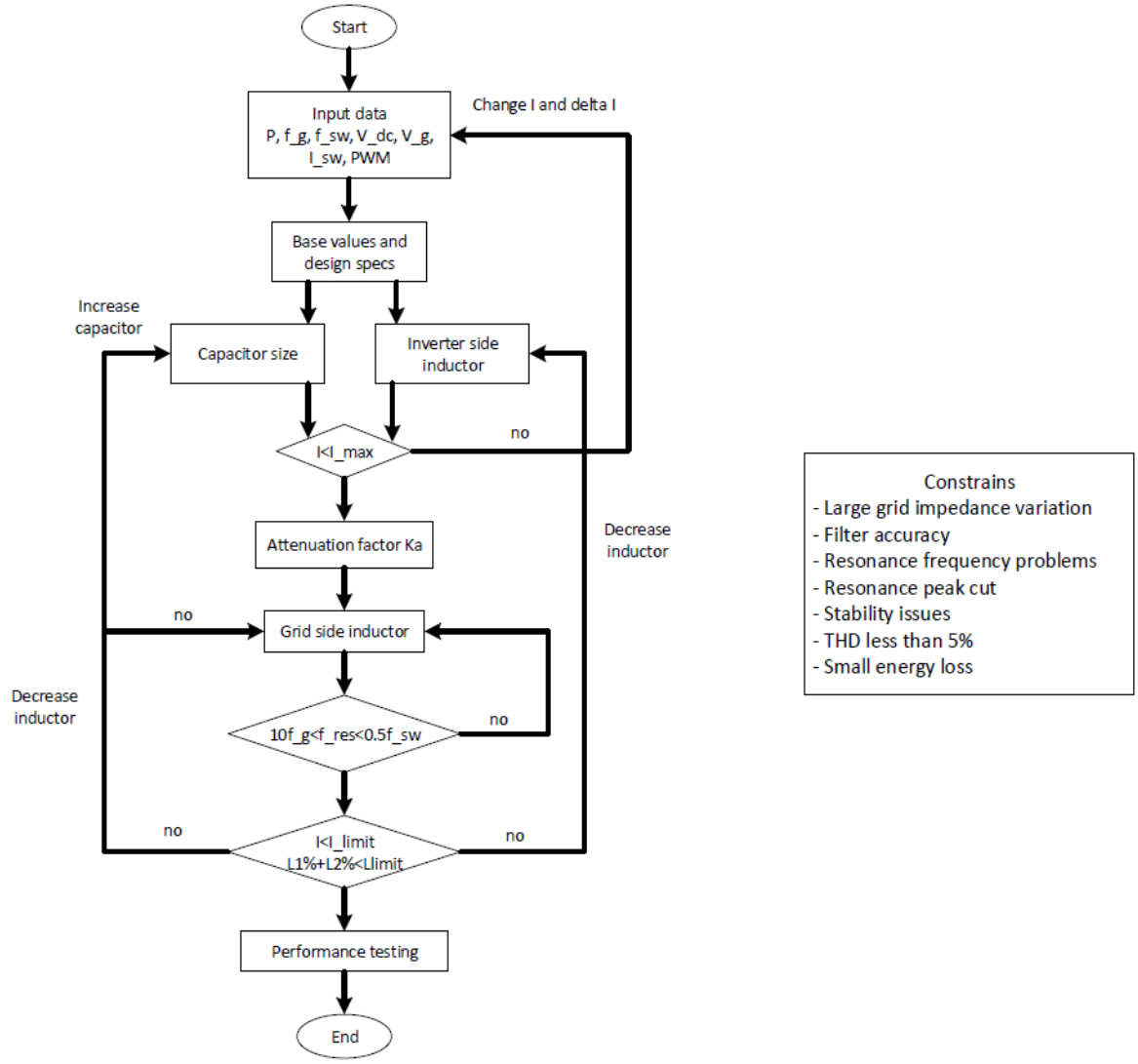

Figure 3 LCL filter coefficients design procedure.

2.1.2 LCL Filter with Damping Resistor Design

The main problems with LCL filters are control input weakening and output wavering caused by resonance. Components and parameters of the filter design significantly affect the resonance size and frequency.

The most common stabilization method is to add a damping resistor in series R_d with the capacitor to suppress the resonance. When this resistor is added, the quality factor $Q = R_d\sqrt{\frac{C}{L}}$ is taken into account, which also introduces a zero to the previous transfer function.

The transfer function of the LCL filter with damping resistor in (5) can be rewritten in terms of Q in (13). By comparing (7), we can see that the multiple roots now become a pair of conjugate roots. The addition of one negative zero causes a turning point on the Bode figure of +20dB/dec of magnitude and +45 degrees of the phase.

$$Y(s) = \frac{\sqrt{LC}Qs + 1}{s(L_1 + L_2)\left(LCs^2 + \sqrt{LC}Qs + 1\right)} \tag{13}$$

2.1.3 Damping Resistor Design Constraints

The most important criterion for designing this passive damping filter is that it does not affect any other part of the grid. Therefore, the stability of the control system should be guaranteed first. In addition, the following points need to be noted in the design:

- Admittance peak: The higher the admittance peak, the smaller the control input and the larger the output fluctuations, so this peak needs to be lowered. The capacitance and inductance in the system will cause the admittance peak to increase, so we try to reduce the size of these parts.
- Frequency response: The resonance frequency depends on the size and the type of damping elements, so it is important to choose damping parameters carefully. The filter size and impedance determine the frequency shift, so impedance calculation also needs to be considered in the design. The resistance in the system will increase the damping frequency, reduce high-frequency decay, and display a characteristic frequency that varies.
- Efficiency: An increase in the filter size, especially the capacitance, will lead to an increase in the current through it, which will increase the power loss and lead to low efficiency.

2.2 Optimal Design Procedure

The design aim is to reduce the admittance peak at the resonance frequency, depress the high frequency, and limit the power loss. The design consists of three parts: main filter parameter design, damping elements optimization, circuit stability test. In general, the initial values are selected first and then adjusted continuously to ensure the dynamic stability, harmonics limit, suitable phase margin and gain margin, lowered admittance peak, and less power loss.

2.2.1 Main LCL Filter Parameter Design

The leftward inductance L_1 is calculated using ripple current. The capacitor C percentage is limited to 5% in order to ensure a good power factor and large fundamental current. The filter attenuation determines the inductance L_2. Also, all the selected values need to satisfy (6) and (9).

2.2.2 Damping Elements Design

The transfer function of the PR controller in continuous time is (14). At 50Hz (314 rad/s), the gain of the amplitude-frequency curve is infinite, which is why the proportional resonant controller can track a particular frequency signal without static error. However, in practical applications, the reference given frequency is often not a fixed constant. For example, the grid frequency may vary from 49.5Hz to 50.5Hz, so the quasi-proportional resonance control is often used.

$$G_c(s) = K_p + \frac{K_r s}{s^2 + {w_r}^2} \tag{14}$$

The transfer function from the output voltage of inverter to grid side current is,

$$G_{i2}(s) = \frac{i_2}{v_1} = \frac{1}{sL_1} \frac{{\gamma_{LC}}^2}{(s^2 + {w_{res}}^2)} \tag{15}$$

where $\gamma_{LC} = \sqrt{\frac{1}{L_2 C}}$.

The transfer function of the inverter with PWM could be,

$$G_{inv}(s) = e^{-sT_d} V_{DC} |k_{PWM}| \tag{16}$$

If sampled with time delay using zero-order hold, then the delay time with sample time T_s is,

$$G_{delay}(s) = \frac{1 - e^{-sT_s}}{sT_s} \tag{17}$$

So that the forward open loop transfer function of the system is,

$$G_o(s) = G_{inv}(s) G_c(s) G_{i2}(s) \tag{18}$$

With their corresponding delay $G_{i2}(s)$. The unity feedback closed loop using Mason's gain formula is,

$$\mathrm{H}(s) = \frac{G_o(s)}{1 + G_o(s)} \tag{19}$$

In the bode plot of the LCL filter without the damping resistor, the controller gains are hard to be designed, due to the large resonance amplitude and dramatic phase conversion through -180°. The adding of damping resistor not only softens this transition but also cut resonance peak magnitude. Then the controller gains are designed more appropriately. By finding the crossover frequency prior to resonance frequency and choosing damping resistors, this loop gains could be calculated. The phase here is lower than -180° so that the sharp peak will not influence the stability feature. That is, no Nyquist encirclement of -1 point. The frequency could be calculated at the point where the phase of forward path goes to -180°.

$$\angle e^{-jwh} G_{inv}(jw) G_c(jw) G_{i2}(jw) = -\pi \tag{20}$$

LCL filter resonance has negligible effect on phase response. Controller resonance frequency is more than a decade below the crossover frequency, so also making little contribution, namely $\angle G_c(jw) \approx 0$. The LCL filter makes contribution only at resonance frequency, so that the angle $\angle G_{i2}\left(e^{-jwh}\right)$ reduces to $\angle G_{i2}\left(\frac{1}{e^{-jwh}} - 1\right)$. With fixed LCL values, this optimized damping resistance design will significantly adjust this frequency domain bode response. The main design idea is to use the optimized cost function and find the optimal Q_{opt} making least resonance peak and lowest high frequency component in bode plot.

Figure 4 shows the inversely proportional relationship between Q and the dB magnitude $20log_{10}(|G_o(jw_{res})|)$ at the resonant frequency. The existence of Q can significantly reduce the resonance peak, but when Q increases to a certain value, the resonance peak is completely reduced. By responding at the resonant frequency, we need as large a Q as possible to offset the damping.

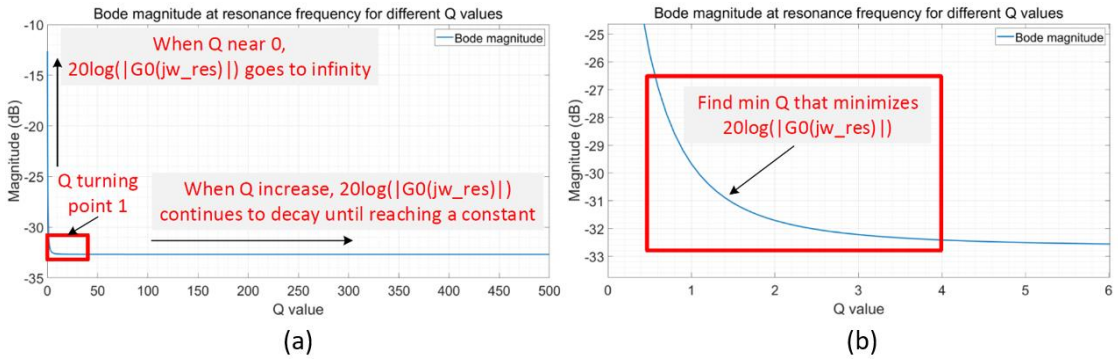

Figure 4 (a) Magnitude with Q value relationship when frequency at resonance frequency. **(b)** Zoomed in display of magnitude with Q value relationship when frequency at resonance frequency.

At the same time, the warping in the high frequency part needs to be suppressed. The relationship between Q and amplitude of the high frequency part $20log_{10}(|G_o(jw_{inf})|)$ is drawn in Figure 5. Obviously, when Q is zero, the high frequencies are lowest. As Q increases, the amplitude must rise. Then the lowest high frequency amplitude should be found when the resonance allows. This requires a compromise. In terms of energy loss, Q also should not be too large.

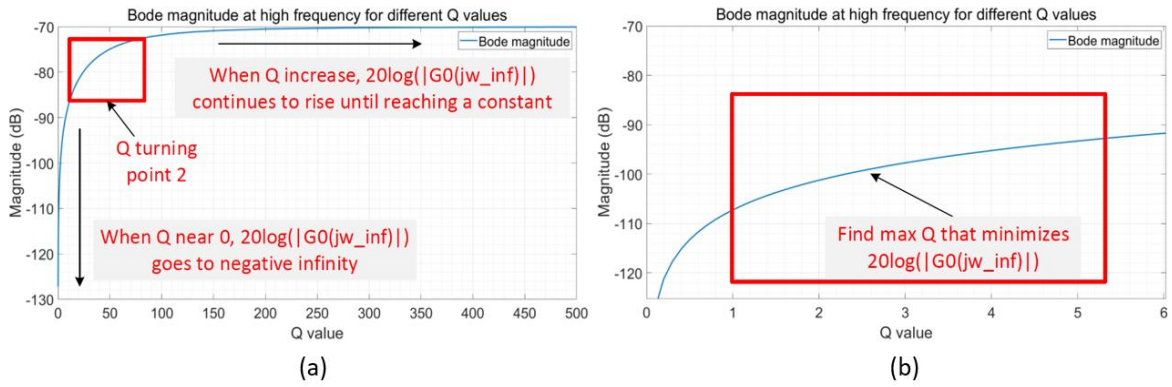

Figure 5 (a) Magnitude with Q value relationship when frequency at high frequency. **(b)** Zoomed in a display of magnitude with Q value relationship when frequency at high frequency.

The optimization algorithm is with cost function:

$$J \coloneqq \sum_{k=0}^{N_f} argmin\left(inv(\|G_o(jw_{res})\| * \|G_o(jw_{+\infty})\|)\right) \tag{21}$$

where the initial condition $Q(0) = Q_0$, the optimal quality factor $Q = Q_{opt}$ could be found for time k=0,1,…N_f till the final time. According to the optimality principle, this optimal Q is also the optimal solution over any subinterval during the whole time period. Usually, the range of Q is around 0 to 5. But in this algorithm, a wider range is tested from 0 to 500.

Also, this is making $Q = Q_{opt}$ with optimal resistance. Several aspects affect each other and determine the selection of damping parameters.

- Admittance peak: The stability and admittance peak of the open-loop system can be seen from the Nyquist diagram and the root locus plot in later simulation plots. Smaller Q increases the admittance peak, and larger Q continues to decrease the admittance peak until it reaches a fixed value, as shown in Figure 6.

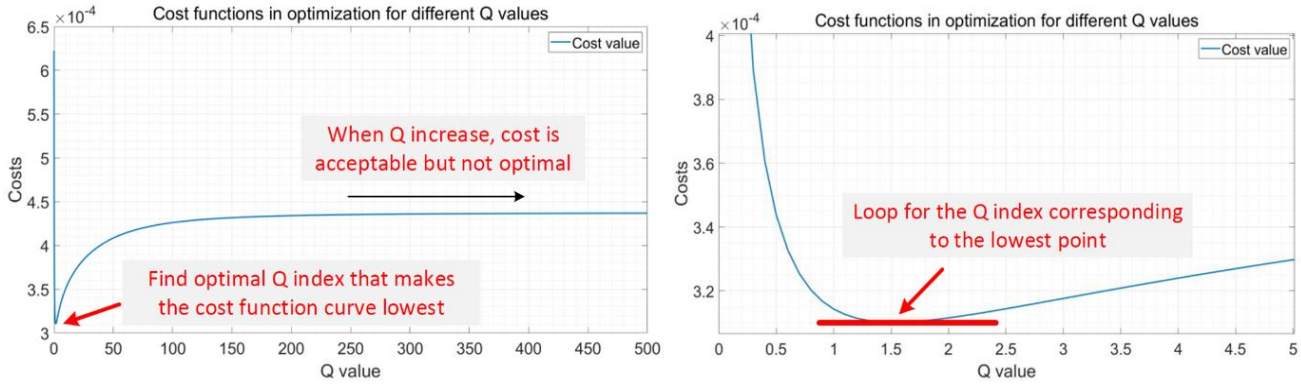

Figure 6 (a) Optimized cost function for Q finding algorithm. **(b)** Zoomed in display of optimized cost function for Q finding algorithm.

- Frequency response: The above range of Q can weaken the decay of the high frequency part of in frequency response. That is, it's lifting up the high frequency part at around 20dB/decade that was decaying. Frequency response also shows that the harmonic proportions are limited.
- Efficiency: Larger Q results in an increase in both current and damping loss. It is necessary to have smaller Q , a small capacitor, or a large capacitor separated in parallel. In this way, both currents through each branch and total loss are diminished

Optimal calculation simplicity: Q decides the optimization, so Q is adjusted when ensuring the stability and not worsening the effect of other parts of the filter. According to Figure 7, optimal quality factor Q is found. The optimal damping resistor is calculated using (22) and (23).

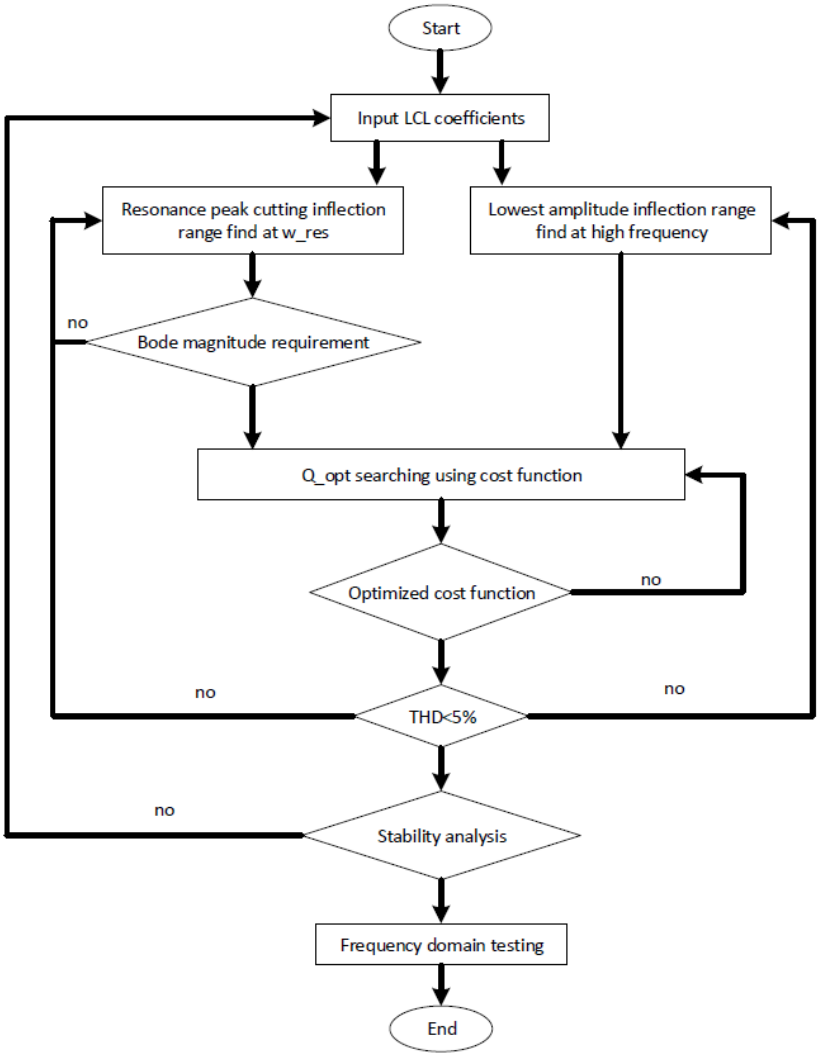

Figure 7 Proposed quality factor optimization algorithm.

$$R_d = R_0 Q_{opt} \tag{22}$$

$$R_0 = \sqrt{\frac{L}{C}} \tag{23}$$

In the procedure below, the aforementioned LCL coefficients are used. Two targets are optimized to satisfy the minimum cost function requirement: the resonance peak cutting at resonance frequency, and the lowest amplitude at high frequency. For each object, the bode plot is checked to find the lowest point. Later, the optimal quality factor is calculated. Putting this optimal value back into the cost function to test the optimized result. Finally, three aspects are used to verify its filtering, stability and optimality: the voltage and current THD, the stability analysis, and the frequency domain response.

2.2.3 Circuit Stability Test

Stability is detected under extreme conditions. If the edges are stable, the parameters selected within this range make the system stable. The tested extreme cases contain small loads, large bus

impedance, and large tolerance in passive elements. Results can be seen from the simulated root locus plot.

3. Simulation

Simulations are conducted in MATLAB/Simulink. The AC microgrid system used is a second-order system, shown in Figure 8, with two breakers switched on and off at a certain time. Several cases are studied to prove the feasibility and optimality of the proposed method.

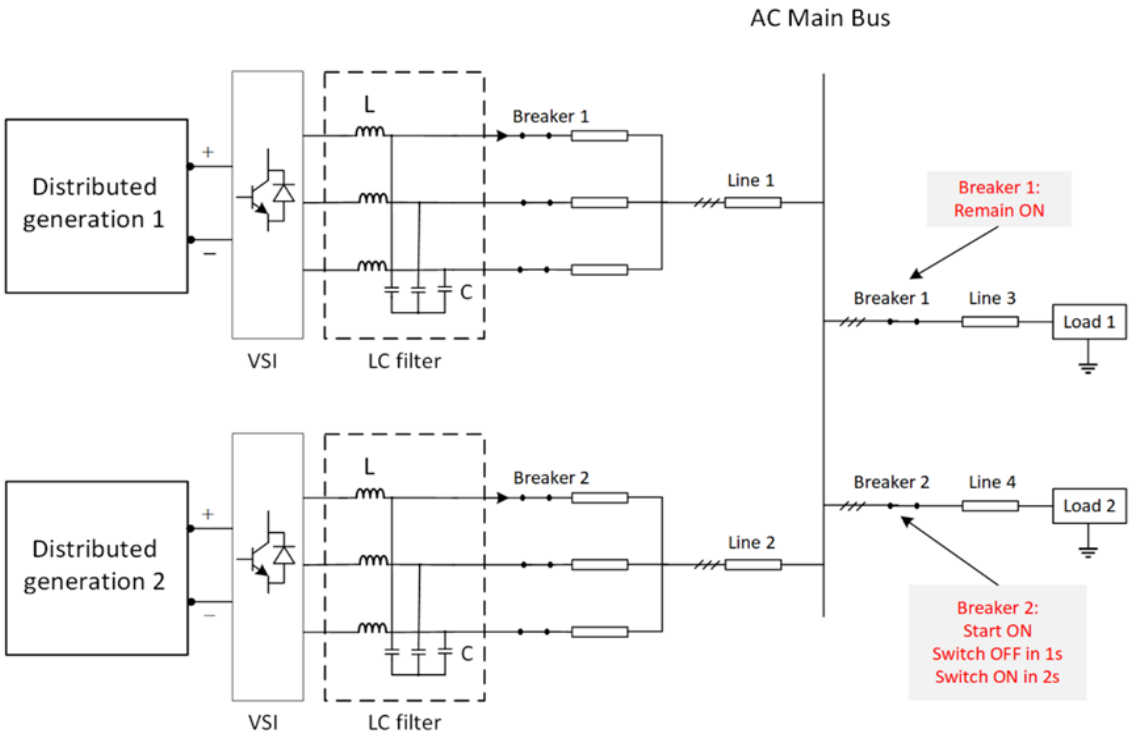

Figure 8 Second-order islanded AC microgrid system used in the simulation.

The parameters used in MATLAB/Simulink simulation are listed in Table 2.

Table 2 Microgrid system parameters.

Parameters	Value
Nominal frequency	50 Hz
Nominal voltage in DC subsystem	800 V
Nominal voltage in AC subsystem	415V
Distributed generation 1 active power	12×10^3 W
Distributed generation 1 reactive power	0 Var
Distributed generation 2 active power	12×10^3 W
Distributed generation 2 reactive power	0 Var
Load 1 active power	20×10^3 W

Parameters	Value
Load 1 reactive power	3×10^3 Var
Load 2 active power	5×10^3 W
Load 2 reactive power	1.2×10^3 Var
Distributed generation inner resistance	1×10^{-4} Ohm
Distributed generation inner inductance	1×10^{-5} H
Branch resistance	1×10^{-5} Ohm
Branch inductance	1×10^{-9} H
LCL filter capacitance	2.5×10^{-5} F
LCL filter inductance at inverter side	2×10^{-3} H
LCL filter inductance at load side	1×10^{-4} H
LCL filter R_0	1.95 Ohm

Four cases are studied. Case 1 and case 2 are two extreme conditions used to compare with the case where there is no optimal algorithm. Case 3 is the optimized damping resistor from the method of $w_0 = w_{inf}$ in [1]. And case 4 is our proposed optimization method.

Table 3 Case studies.

Cases	Condition	Q value	Rd
1	Minimal condition case	0	0
2	Maximum condition case	Inf	Inf
3	Frequency based optimization case [1]	3	$3 * \mathrm{R}_0$
4	Proposed optimization case	1.5	$1.5 * \mathrm{R}_0$

3.1 System Stability Analysis

Stability characteristics are studied under the conditions of a typical filter and optimized filter. By comparing whether the optimal filter is added, the change of system properties can be obtained, which can also be used to adjust system parameters in the future.

The root locus diagram is used to observe the position of the roots of the open-loop system and to locate those of the closed-loop system. By looking at the motion trace of the roots, especially the locations of the desired roots in the MATLAB dynamic diagram, we can configure the positions of the closed-loop poles according to the specific parameter requirements.

For example, in the MATLAB dynamic diagram, we can find the root positions that limit the phase margin, bandwidth, steady-state error, response time, and overshoot. Root locus plot in Figure 9 and Nyquist plot in Figure 10 present extreme cases stability test in open loop systems. As mentioned above, the best case with optimal damping resistor, the worst case with zero damping resistor, and the worst case with larger damping size are plotted. Q_{opt1} is the optimized Q from case

3, and Q_{opt2} is the optimized Q from case 4. An ideal figure has an optimal damping ratio of $\frac{\sqrt{2}}{2}$. The other two worst case scenarios tend to be marginally stable or unstable.

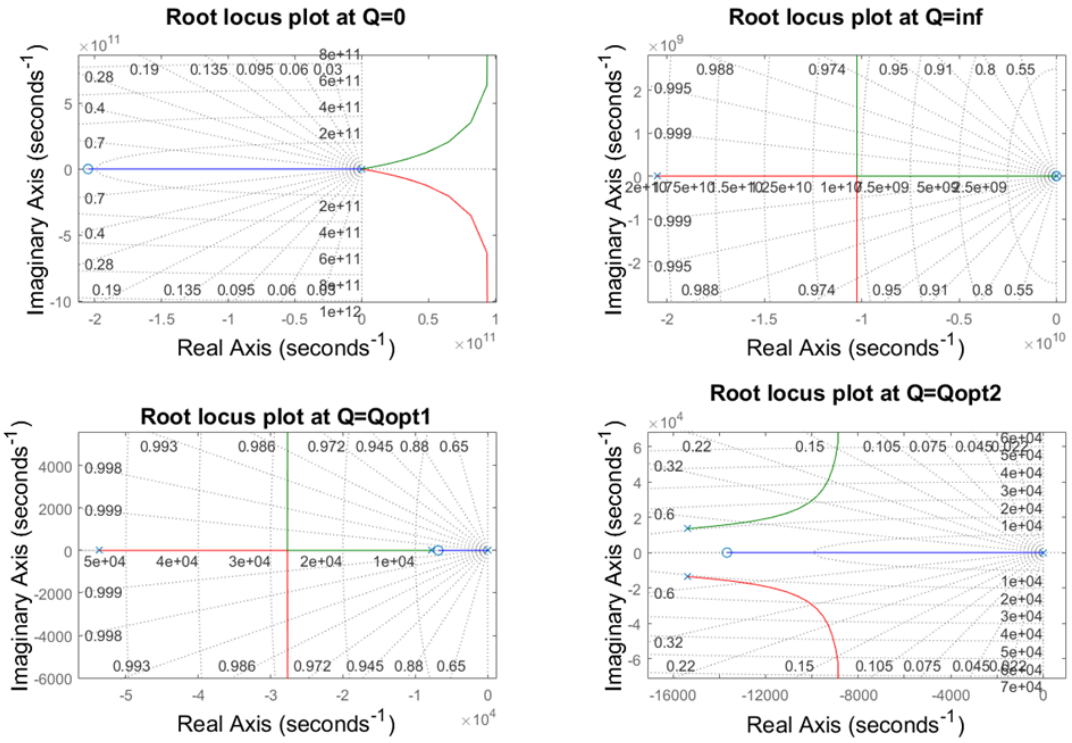

Figure 9 Root locus plot for all cases.

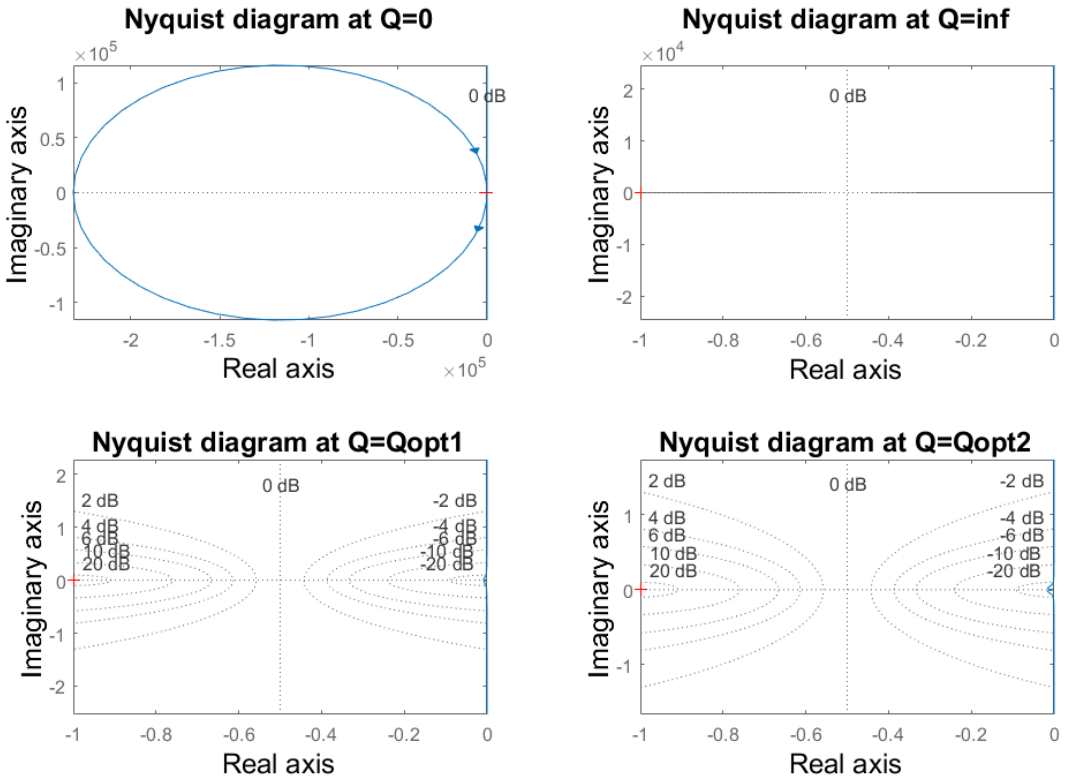

Figure 10 Nyquist diagrams for all cases.

3.2 Simulation Results

3.2.1 System Response in the Time Domain

Figure 11-13 present system responses using LCL filter and LCL filter with optimized damping elements in terms of grid voltage, active power, and reactive power. It can be found by looking at the figure that the system response speed is not significantly affected by the selected filter, but the degree of smoothness is not the same. However, the effect of the filters is not quite clear in the time domain, and other data processing analysis is needed.

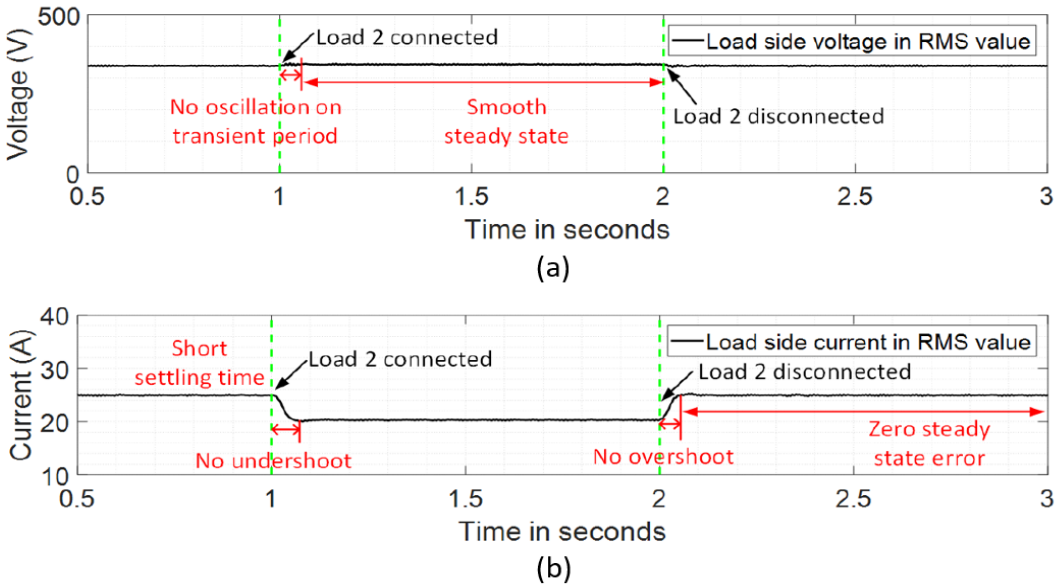

Figure 11 System load side voltage **(a)** and current **(b)** responses in magnitude.

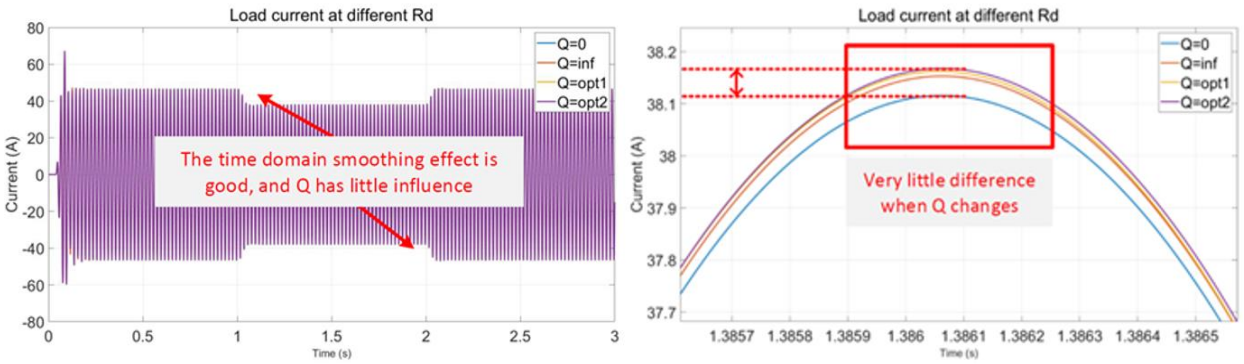

Figure 12 (a) System load side current responses for all cases. **(b)** Zoomed in display of system load side current responses for all cases.

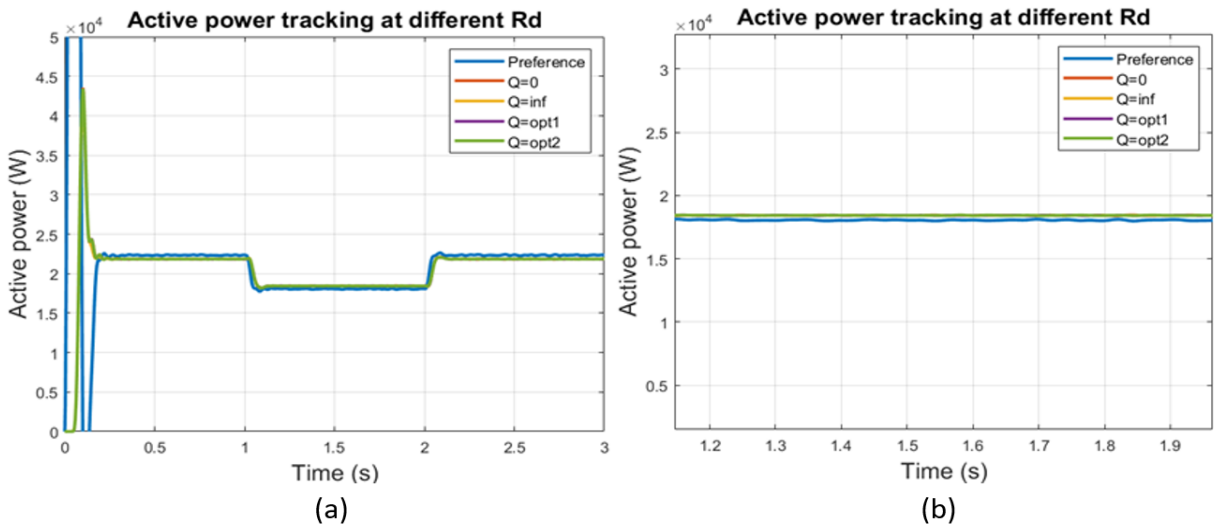

Figure 13 (a) System active power tracking behavior for all cases. **(b)** Zoomed in a display of system active power tracking behavior for all cases.

In the THD comparison, all of the cases show good results, all within the acceptable range. It seems THD works best as Q goes to infinity, which is not realistic. Only by sacrificing part of the THD effect can we get the best amplitude reduction effect in the frequency domain [42].

Table 4 THDs of voltage and current.

THD	Value
Current THD when Q=0	1.81%
Current THD when Q=inf	1.69%
Current THD when Q=Qopt1	1.83%
Current THD when Q=Qopt2	1.83%
Voltage THD when Q=0	1.85%
Voltage THD when Q=inf	1.73%
Voltage THD when Q=Qopt1	1.89%
Voltage THD when Q=Qopt2	1.88%

3.2.2 Frequency Response under Different Quality Factor Selection

It can be seen from Figure 14 that the low frequency and admittance peak responses are similar regardless of the value of Q. The difference is the degree of weakening at the high frequencies. In the low frequency part, the slopes are the same whether the resistance is added or not because this is the inductance characteristic curve caused by the inductances. The main differences are at the admittance peak and the high frequency part. For some types of filters, this damping resistor will leave the low and high frequencies unchanged, only reducing the admittance peak.

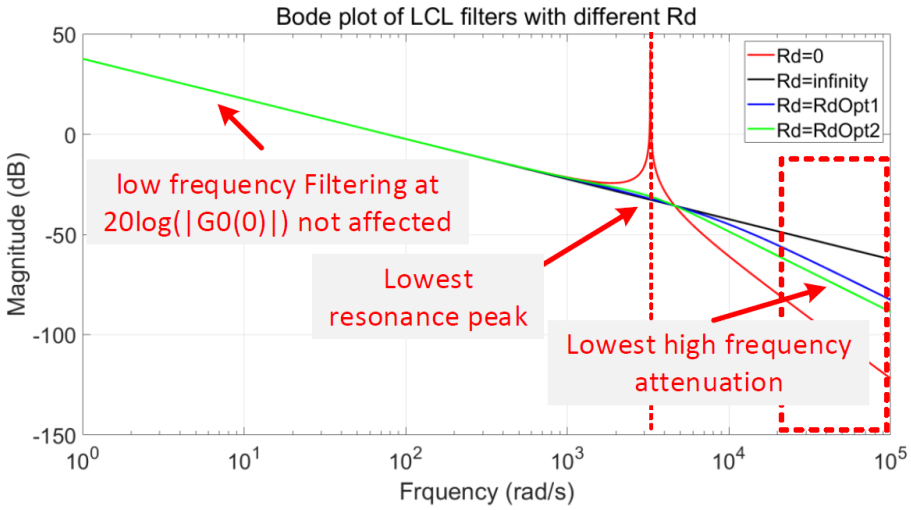

Figure 14 Bode plots for all cases.

At low frequencies, the slope is 20dB/decade. Filter admittance peak of the LCL filter with optimal damping resistor is flattened, while that of only LCL filter exhibits a sharp peak; At the peak of admittance, the amplitude is greatly weakened by the addition of this damping resistor, which can make up for the shortcoming of high frequency impairing.

High frequency part of the LCL filter has 60dB/decade, while that of the LCL filter with optimal damping resistor is tuned to 40dB/decade. The degree of weakening in decay varies according to the LCL filter parameters selection. And this proposed optimization result is the best among all selected damping resistor parameters:

- When $Q = 0$, no damping resistor is added, so the high frequency decay remains invariant and lowest.
- When Q goes to infinity, the high frequency asymptote goes up to a constant, which is the highest position possible.
- When Q is the optimal value, the high frequency decay is reduced by 20dB/decade. Our proposed method has an even lower magnitude at high frequency than the other optimization method.

Therefore, the optimal damping resistor can ensure that the high-frequency response is also optimally weakened in the case of the same admittance peak reduction.

3.2.3 System Response in the Spectrum Diagram

The frequency response result of the system in Figure 15 proves the previous theory in the aspect of harmonics. It is clear that as long as there is damping resistance, harmonics will increase. However, in terms of making harmonics grow, the proposed optimization method is superior. Because of its efforts to push down the harmonics, it is closest to a none damping resistance case.

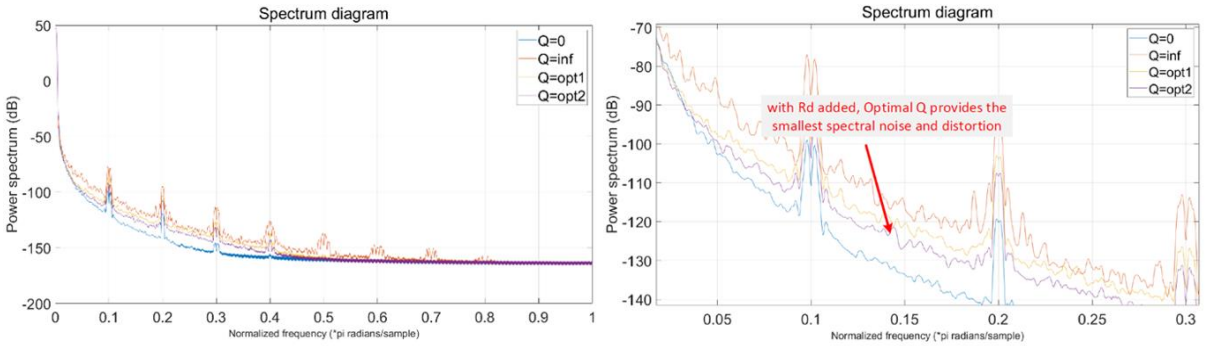

Figure 15 (a) System Fourier transformed spectrum response for all cases. **(b)** Zoomed in display of system Fourier transformed spectrum response for all cases.

4. Conclusions

The passive damping optimization method proposed in this paper has the advantages of reducing admittance peak, attenuating high frequency component, low damping loss, and high efficiency. By testing different Q parameters, it is proved that this selection has the optimal effect in THD, FFT and bode plots. The V-P control power tracking method under constant frequency simplifies the calculation while getting efficient tracking. In order to avoid wasting time, the optimal parameters (optimal frequency, optimal quality factor, optimal damping resistor) are obtained directly through the formula of the filter design process in this paper.

Some key findings from the results are:

- System stability and time-domain power traceability are always maintained.
- The adjustment of the damping resistance is so small that the output amplitude in time domain response is affected.
- The total harmonic distortion is kept within 1.90%, while the optimal damping resistor gives the lowest amplitude on the spectrum diagram among all cases with damping resistor added.
- Under the condition of keeping the low frequency amplitude constant, the amplitude reduction on the resonant frequency is the lowest, and the high frequency amplitude is also guaranteed to be the lowest among all cases involving the damping resistance.
- Compared with the existing single-object optimization algorithms, this algorithm adds optimization of two frequency bands, and has multiple restrictions and verification to ensure that the system can achieve the expected optimal effect.

Results show that this LCL filter parameter design procedure is feasible. Furthermore, the optimal design of the damping resistor satisfies the reduction of the admittance peak, the rationality of the frequency domain response and the high efficiency of the system output. The amplitudes at resonance peak and high frequency components are both flattened and lowered. Future system optimization might focus on filter type selection, controller optimization and dynamics prediction.

Author Contributions

Xiuhui Tang: methodology, manuscript writing, simulation, data analysis; Daming Zhang: academic guidance, model design, organization, implementation, reviewing; Hua Chai: calculations, investigation, data analysis, reviewing and editing.

Competing Interests

The authors have declared that no competing interests exist.

References

1. Beres RN, Wang X, Blaabjerg F, Liserre M, Bak CL. Optimal design of high-order passive-damped filters for grid-connected applications. IEEE Trans Power Electron. 2015; 31: 2083-2098.
2. Liserre M, Blaabjerg F, Hansen S. Design and control of an LCL-filter-based three-phase active rectifier. IEEE Trans Ind Appl. 2005; 41: 1281-1291.
3. Djema MA, Boudour M, Agbossou K, Cardenas A, Doumbia ML. Optimized PID for direct power control with an improved LCL filter design using GWO for three-phase inverters. Proceedings of the 2018 International conference on electrical sciences and technologies in Maghreb (CISTEM); 2018 October 28-31; Algiers, Algeria. Piscataway Township: IEEE. p.1-6.
4. Liu Y, Jiang S, Jin D, Peng J. Performance comparison of Si IGBT and SiC MOSFET power devices based LCL three-phase inverter with double closed-loop control. IET Power Electron. 2019; 12: 322-329.
5. Giacomini JC, Michels L, Pinheiro H, Rech C. Design methodology of a passive damped modified LCL filter for leakage current reduction in grid-connected transformerless three-phase PV inverters. IET Renew Power Gener. 2017; 11: 1769-1777.
6. Bolsens B, De Brabandere K, Van den Keybus J, Driesen J, Belmans R. Model-based generation of low distortion currents in grid-coupled PWM-inverters using an LCL output filter. IEEE Trans Power Electron. 2006; 21: 1032-1040.
7. Jalili K, Bernet S. Design of LCL filters of active-front-end two-level voltage-source converters. IEEE Trans Ind Electron. 2009; 56: 1674-1689.
8. Rockhill AA, Liserre M, Teodorescu R, Rodriguez P. Grid-filter design for a multimegawatt medium-voltage voltage-source inverter. IEEE Trans Ind Electron. 2010; 58: 1205-1217.
9. Xu J, Xie S. LCL-resonance damping strategies for grid-connected inverters with LCL filters: A comprehensive review. J Mod Power Syst Clean Energy. 2018; 6: 292-305.
10. Xia W, Kang J. Stability of LCL-filtered grid-connected inverters with capacitor current feedback active damping considering controller time delays. J Mod Power Syst Clean Energy. 2017; 5: 584-598.
11. Wang X, Blaabjerg F, Wu W. Modeling and analysis of harmonic stability in an AC power-electronics-based power system. IEEE Trans Power Electron. 2014; 29: 6421-6432.
12. Sun J. Small-signal methods for AC distributed power systems–a review. IEEE Trans Power Electron. 2009; 24: 2545-2554.
13. Holmes DG, Lipo TA, Mcgrath BP, Kong WY. Optimized design of stationary frame three phase AC current regulators. IEEE Trans Power Electron. 2009; 24: 2417-2426.
14. Wang X, Blaabjerg F, Loh PC. Grid-current-feedback active damping for LCL resonance in grid-connected voltage-source converters. IEEE Trans Power Electron. 2015; 31: 213-223.
15. Yepes AG, Freijedo FD, López O, Doval-Gandoy J. High-performance digital resonant controllers implemented with two integrators. IEEE Trans Power Electron. 2010; 26: 563-576.
16. Semasa M, Kato T, Inoue K. A simple and effective time delay compensation method for grid-connected inverter with an LCL filter: Application to active damping method. Proceedings of

the 2017 IEEE 18th workshop on control and modeling for power electronics (COMPEL); 2017 July 9-12; Stanford, CA, USA. Piscataway Township: IEEE.

17. Chtouki I, Zazi M, Feddi M, Rayyam M. LCL filter with passive damping for PV system connected to the network. Proceedings of the 2016 International renewable and sustainable energy conference (IRSEC); 2016 November 14-17; Marrakech, Morocco. Piscataway Township: IEEE.
18. Wu W, Liu Y, He Y, Chung HS, Liserre M, Blaabjerg F. Damping methods for resonances caused by LCL-filter-based current-controlled grid-tied power inverters: An overview. IEEE Trans Ind Electron. 2017; 64: 7402-7413.
19. Wu TF, Misra M, Lin LC, Hsu CW. An improved resonant frequency based systematic LCL filter design method for grid-connected inverter. IEEE Trans Ind Electron. 2017; 64: 6412-6421.
20. Wu W, Sun Y, Huang M, Wang X, Wang H, Blaabjerg F, et al. A robust passive damping method for LLCL-filter-based grid-tied inverters to minimize the effect of grid harmonic voltages. IEEE Trans Power Electron. 2013; 29: 3279-3289.
21. Pena-Alzola R, Liserre M, Blaabjerg F, Sebastián R, Dannehl J, Fuchs FW. Analysis of the passive damping losses in LCL-filter-based grid converters. IEEE Trans Power Electron. 2012; 28: 2642-2646.
22. Channegowda P, John V. Filter optimization for grid interactive voltage source inverters. IEEE Trans Ind Electron. 2010; 57: 4106-4114.
23. Beres R, Wang X, Blaabjerg F, Bak CL, Liserre M. A review of passive filters for grid-connected voltage source converters. Proceedings of the 2014 IEEE applied power electronics conference and exposition – APEC 2014; 2014 March 16-20; Fort Worth, TX, USA. Piscataway Township: IEEE.
24. Ögren J. PLL design for inverter grid connection: Simulations for ideal and non-ideal grid conditions. Uppsala, Swedish: Uppsala University; 2010.
25. Reznik A, Simões MG, Al-Durra A, Muyeen SM. LCL filter design and performance analysis for grid-interconnected systems. IEEE Trans Ind Appl. 2013; 50: 1225-1232.
26. Tran TV, Yoon SJ, Kim KH. An LQR-based controller design for an LCL-filtered grid-connected inverter in discrete-time state-space under distorted grid environment. Energies. 2018; 11: 2062.
27. Gui Y, Wang X, Blaabjerg F. Vector current control derived from direct power control for grid-connected inverters. IEEE Trans Power Electron. 2018; 34: 9224-9235.
28. Zhang D. Operation of microgrid at constant frequency with a standby backup grid-forming generator. Proceedings of the 2016 IEEE international conference on Power System Technology (POWERCON); 2016 September 28 - October 1; Wollongong, NSW, Australia. Piscataway Township: IEEE.
29. Zhang D, Fletcher J. Operation of autonomous AC microgrid at constant frequency and with reactive power generation from grid-forming, grid-supporting and grid-feeding generators. Proceedings of the TENCON 2018 – 2018 IEEE region 10 conference; 2018 October 28-31; Jeju, Korea (South). Piscataway Township: IEEE.
30. Tang X, Zhang D. Islanded AC microgrid stability and feasibility analysis on VP control with estimation at constant frequency. Proceedings of the 2019 9th International conference on power and energy systems (ICPES); 2019 December 10-12; Perth, WA, Australia. Piscataway Township: IEEE.

31. Zhang D. Issues on load shedding in a microgrid operated at constant frequency. Proceedings of the 2017 20th International conference on electrical machines and systems (ICEMS); 2017 August 11-14; Sydney, NSW, Australia. Piscataway Township: IEEE.
32. Kundur P. Power system stability and control. New York: McGraw-Hill; 1993.
33. Dorf RC, Bishop RH. Modern control systems. Boston: Pearson; 2011.
34. Said-Romdhane MB, Naouar MW, Belkhodja IS, Monmasson E. An improved LCL filter design in order to ensure stability without damping and despite large grid impedance variations. Energies. 2017; 10: 336.
35. Guan Y, Xie Y, Wang Y, Liang Y, Wang X. An active damping strategy for input impedance of bidirectional dual active bridge DC–DC converter: Modeling, shaping, design, and experiment. IEEE Trans Ind Electron. 2020; 68: 1263-1274.
36. Poongothai C, Vasudevan K. Design of LCL filter for grid-interfaced PV system based on cost minimization. IEEE Trans Ind Appl. 2018; 55: 584-592.
37. Xu J, Xie S, Huang L, Ji L. Design of LCL-filter considering the control impact for grid-connected inverter with one current feedback only. IET Power Electron. 2017; 10: 1324-1332.
38. Dursun M, Döşoğlu MK. LCL filter design for grid connected three-phase inverter. Proceedings of the 2018 2nd International symposium on multidisciplinary studies and innovative technologies (ISMSIT); 2018 October 19-21; Ankara, Turkey. Piscataway Township: IEEE.
39. El Boubakri A. Analysis of the performance of droop controlled inverters in mini-grids. Montreal, Quebec, Canada: Concordia University; 2013.
40. Kahlane AE, Hassaine L, Kherchi M. LCL filter design for photovoltaic grid connected systems. J Renew Energ. 2014; 227-332.
41. Mahamat C, Petit M, Costa F, Marouani R, Mami A. Optimized design of an LCL filter for grid connected photovoltaic system and analysis of the impact of neighbors' consumption on the system. J Electr Syst. 2017; 13: 618-632.
42. Zhang D, Dutta R. Application of partial direct-pole-placement and differential evolution algorithm to optimize controller and LCL filter design for grid-tied inverter. Proceedings of the 2014 Australasian universities power engineering conference (AUPEC); 2014 September 28 - October 1; Perth, WA, Australia. Piscataway Township: IEEE.